Acoustically induced current flow in graphene

V. Miseikis, J. E. Cunningham,[a] K. Saeed, R. O'Rorke, and A. G. Davies
School of Electronic and Electrical Engineering, University of Leeds, Woodhouse Lane, Leeds LS2 9JT, United Kingdom

(Received 30 January 2012; accepted 2 March 2012; published online 27 March 2012)

We demonstrate the directed control of charge carriers in graphene using the electric field that accompanies the propagation of surface acoustic waves (SAWs) on a piezoelectric surface. Graphene grown by chemical vapor deposition was transferred to the surface of lithium niobate, allowing its direct integration with interdigital transducers used for SAW generation and detection. Radio frequency (RF) signal applied to the transducers at their resonant frequency was found to generate a direct current flow by the transport of p-type charge carriers. The acoustically induced current scales linearly with the applied RF power and can be observed even in presence of a counter-flow current induced by an applied bias. © *2012 American Institute of Physics*. [http://dx.doi.org/10.1063/1.3697403]

The interaction between surface acoustic waves (SAWs) and carriers confined in semiconductor low-dimensional systems (LDSs) has been studied extensively since the early 1990s, revealing a wealth of physics. Two classes of effects are typically studied. The first is the effect of the charge carriers on the SAW propagation, where the attenuation and velocity modulation of the acoustic signal can be used to determine the conductivity of the LDS. This effect has been used, for example, to demonstrate geometric resonances of composite Fermions in the quantum Hall effect of 2D electron systems, providing early evidence for the existence of these quasi-particles.[1] The second class of effect involves the generation of current (or voltage in open circuit) in the LDS by the SAW (the acoustoelectric effect). The conduction and valence bands of the LDS are periodically modulated by the SAW and momentum is transferred to the charge carriers, which generates a current in the SAW propagation direction.[2–5] This effect has been used to generate quantized acoustoelectric current in depleted 1D channels, whereby single electrons are transported one-by-one.[2,4,5] Such SAW-induced currents provide a route towards a current standard,[6] have been used for light-storage in quantum wells,[7] can drive single-photon emission,[8] and have led to studies of coherent control of electron wavefunctions in suitably patterned LDSs.[9] SAWs have also recently been used to transfer single-electrons between spatially well-separated quantum dots.[10,11]

By contrast, the interaction of SAWs with low-dimensional carbon has received far less attention, despite the wealth of physics worthy of study.[12] Experimental work has mainly focused on studies of charge transport in carbon nanotubes,[13] although the propagation of SAWs in graphene has been investigated theoretically.[14] Experimental work on 2D carbon has been limited to measurements of SAW velocity shift and attenuation caused by graphene-like films produced from chemically reduced graphene oxide,[15,16] rather than acoustoelectric effects. A problem that needs to be overcome for the generation of acoustoelectric currents in 2D carbon is that the screening caused by the high sheet carrier density necessitates the use of a highly piezoelectric material. However, the most prevalent technique used for graphene preparation, that of exfoliation from graphite, is typically performed on SiO_2-coated Si in order to make the graphene visible, but this surface is not piezoelectrically active. A potential route could be a flip-chip arrangement, whereby SAWs propagating on a highly piezoelectric substrate are brought into close proximity to a graphene layer prepared on a separate SiO_2-coated Si substrate. However, our studies of this geometry encountered significant cross-talk problems with the semi-metallic graphene films apparently rectifying the radio frequency (RF) signals applied for SAW generation, masking any acoustoelectric current flow.

In this letter, we demonstrate a different strategy, which has allowed us to observe an acoustoelectric current in graphene. Graphene layers grown by chemical vapour deposition (CVD) are integrated directly onto a highly piezoelectric substrate (lithium niobate). This has enabled clear observation of an acoustoelectric current in graphene at room temperature, which follows the expected dependence on applied RF and power. This methodology opens a route to the fabrication of graphene devices, including laterally pattered 2D carbon, whose electronic properties are controlled by applied surface acoustic waves.

A schematic diagram of the devices used in our work is shown in Figure 1. The devices were fabricated on 128° *Y*-rotated, single-crystal lithium niobate by depositing CVD-grown graphene onto lithium niobate using a poly(methylmethacrylate) (PMMA) transfer technique. This allows the standard fabrication of SAW interdigital transducers (IDTs), using optical lithography onto the chip surface, along with direct current (DC) contact pads to contact the carbon layer, enabling acoustoelectric current measurements to be performed. Pairs of IDTs were fabricated for SAW generation and detection in the crystallographic *X* direction, with a centre-to-centre distance of 4.8 mm. Each IDT consisted of 20 pairs of electrodes for SAW excitation and detection, and 22 unconnected electrodes that act as reflectors (to increase SAW intensity), all defined by photolithography. The width and gap between all electrodes was 7.2 μm in the SAW

[a]Author to whom correspondence should be addressed. Electronic mail: eenjec@leeds.ac.uk.

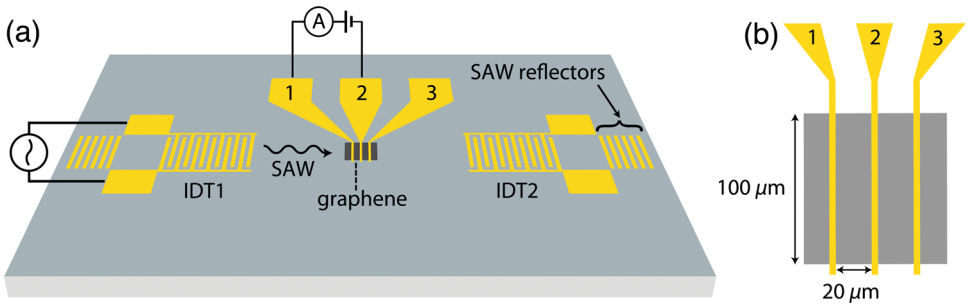

FIG. 1. (a) Schematic diagram of the sample layout, showing etched graphene region deposited on the lithium niobate substrate. (b) Magnification of the central device region showing the numbered contacts and the dimensions of the graphene in an etched device.

propagation direction, while the acoustic aperture of the transducers (set by the overlap between electrodes) was 300 μm. The transducers were aligned so that the electrodes that contact the graphene were located within the acoustic beam path. The periodicity of alternate fingers defines the centre frequency of SAW production; this period was chosen to be 35 μm to produce a centre resonance frequency of $f = v_{saw}/\lambda_{saw} = 114$ MHz, where λ_{saw} is the SAW wavelength and v_{saw} is the SAW propagation velocity (3980 m s^{-1} for the chosen crystal direction).

The graphene was grown on copper foil by CVD as described by Ref. 17 (supplied by Graphene Laboratories Inc.). To release the graphene from copper and position it on the piezoelectric substrate, a PMMA-transfer technique was used.[18] The 20-μm-thick copper foil was drop-coated with PMMA (5% solution in anisole), and then baked for 1 min at 180 °C. The copper was etched away using a 0.0124 M ferric nitrate solution, leaving the graphene attached to the thin PMMA film, floating on the surface of the etch solution. This was rinsed in de-ionized water, transferred to the lithium niobate substrate, and aligned to the centre of the chip. The alignment was possible owing to the good visibility of the PMMA film on lithium niobate. The PMMA film was subsequently dissolved by re-depositing a drop of PMMA-in-anisole solution, and finally removed in acetone.

Four devices were fabricated and measured. Six-electrodes were patterned onto the transferred graphene in the centre of each chip; three electrodes on each side of the SAW path. In devices 1, 3, and 4 the separation between adjacent contacts was 20 μm (defined by optical lithography), whereas device 2 had a fine electrode pattern (defined by electron beam lithography) with contact separation of $\sim$2 μm. Metallization was achieved by electron-beam evaporation of 10 nm of chromium (used as an adhesion layer) followed by 60 nm of gold. In devices 1 and 2, the current was measured by electrodes located at the centre of the region of graphene transferred onto lithium niobate, which was approximately 2×2 mm^2. In device 3 and 4, a 100×100 μm^2 square region of graphene was defined symmetrically around the metal electrodes using optical lithography, with the unwanted carbon outside this region removed by oxygen plasma etching (180 s; 50 W; 0.7 mbar). The geometry of the etched devices is shown in Figure 1(b). All measurements presented are from device 4; data from the other devices is included in the supplemental material,[19] with quantitatively similar results obtained in all four devices.

The 2D nature of the graphene films transferred onto the lithium niobate substrates was confirmed by Raman spectroscopy (using a 633 nm HeNe laser with a spot size of $\sim$5 μm). A typical spectrum is shown in Fig. 2 (similar features were found in all four samples) with prominent symmetrical peaks at $\sim$1390 cm^{-1} (G peak) and $\sim$2700 cm^{-1} (2D peak). The intensity ratio $I_{2D}/I_G \sim 3.3$ is characteristic of single-layer graphene.[17,20] The high intensity of the D peak at $\sim$1350 cm^{-1} indicates significant disorder in all samples measured, which is likely to be caused by the small domain size as well as wrinkles and cracks in the films, as has been seen previously in samples grown by CVD.[18] The selection of higher quality areas was hindered by the low intrinsic visibility of graphene on lithium niobate.

Initially the performance of the SAW transducers was assessed by measuring the S_{21} parameter of each transducer pair using a network analyzer (Agilent E8364B). Figure 3(a) shows the insertion loss of a typical IDT pair fabricated either side of a graphene region. The peak in transmitted power (−15.5 dB) is centered at 111 ± 3 MHz (6 dB bandwidth), corresponding well to the expected value of 114 MHz.

An acoustoelectric current was generated by applying a continuous-wave RF signal to each transducer in turn. The RF signal was generated using a Marconi 2022E unit with Minicircuits ZHL-1–2 W amplifier, which produced a final signal power of +20 dBm, noting that the SAW signal obtained was $\sim$8 dBm smaller owing to losses in the acoustic transduction process, as measured by the transmission measurement. Acoustoelectric current measurements were made using a Keithley 2400-series source-measurement unit

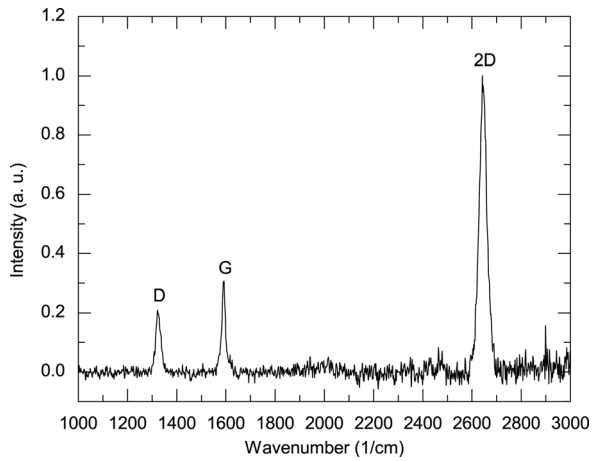

FIG. 2. Raman spectrum of the graphene layer formed on the lithium niobate surface between DC probe contacts showing the characteristic D, G, and 2D peaks. The intensity ratio $I_{2D}/I_G \sim 3.3$ indicates that the signal comes from a single layer of graphene. A background signal from the $LiNbO_3$ substrate has been subtracted.

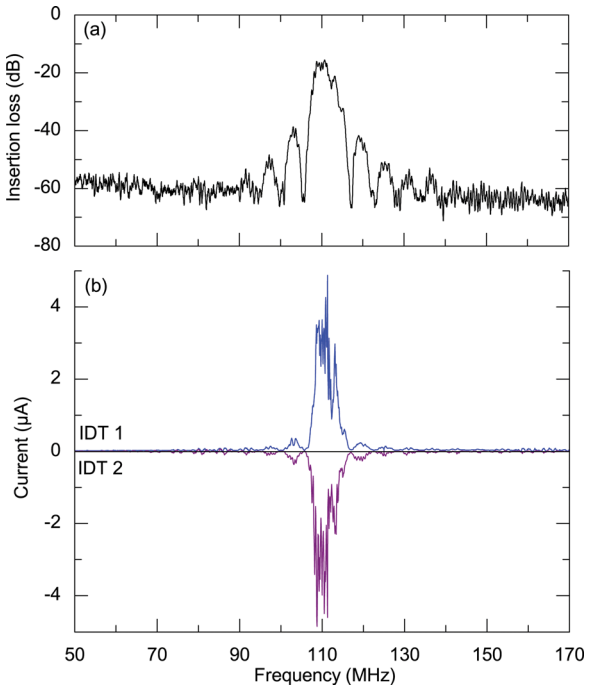

FIG. 3. (a) Transmittance (S_{21}) of a pair of SAW transducers formed either side of a graphene film (device 4). (b) Acoustoelectric current generated between contacts 2 and 3 of device 4 by the two transducers (IDT 1 and IDT 2) with zero bias voltage applied across the graphene film. The DC resistance between the contacts was 970 Ω.

(SMU) between pairs of electrodes contacting the graphene region. In some cases, a small bias of approximately 100 μV was applied across the graphene to offset the burden voltage produced by the SMU output (noting that the acoustically induced currents were several orders of magnitude larger than those generated by this burden voltage).

A peak in current closely following the SAW transmittance response was found for both transducers in all four devices measured (Fig. 3 shows a typical response). Additional current peaks appeared at ~103 MHz and ~120 MHz, corresponding well to the secondary transmittance peaks observed at these frequencies in the SAW response. The direction of acoustoelectric current was determined by which IDT (IDT1 or IDT2) was activated, as expected. In all cases, a positive current flow in the direction of the SAW travel was found indicating hole transport in the graphene. This is as expected from the p-type conduction typically obtained from ambient air-doped graphene films (no annealing was attempted in the current work). To exclude any possible contribution from the underlying substrate, which is of very high DC resistance, we performed a null test between electrodes within the acoustic beam path but disconnected from the graphene. No acoustically induced currents were measured above 50 pA, even for the highest acoustic powers applied, compared with the μA-range acoustoelectric currents measured in graphene. The measured current of several μA is comparable to the values reported previously in hybrid systems, consisting of semiconductor-based 2D electron systems transferred epitaxially to lithium niobate.[21]

The induced current was measured as a function of the RF power applied to each IDT operating at its centre frequency (Figure 4). The peak acoustoelectric current was

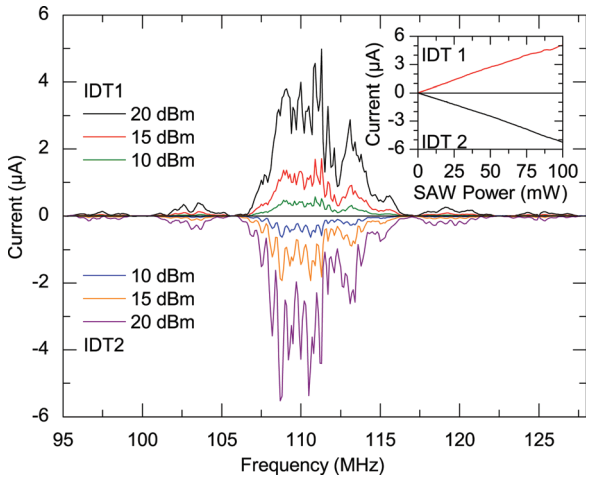

FIG. 4. Acoustoelectric current–frequency traces at different RF power levels applied to each IDT, around the peak in SAW transducer response. Inset: Peak acoustoelectric current as a function of applied power to the two IDTs.

found to vary linearly with RF power, as shown in the inset of Figure 4, in agreement with the current having an acoustoelectric origin.[21] The acoustoelectric measurements were also repeated at different source-drain voltages applied to the graphene layers in the range −10 mV to +10 mV. The applied bias appeared as an offset on the measured acoustoelectric current, as expected (Fig. 5). The acoustic current flow was able to switch the overall current direction at low biases (the timescale of switching being determined by the time taken for SAWs to propagate from the transducer to the graphene— ~0.1 μs for our geometry).

In device 4, the current measurements were repeated between contacts 1-2, 2-3, and 1-3 (see Fig. 1 inset). Despite the similar geometry, a slightly different DC resistance was measured between contacts 1-2 and 2-3 in each device, which could be due to the variations in contact quality and/or levels of disorder in the graphene. The highest acoustoelectric current measured across each region of the device was found to be roughly proportional to the conductance of

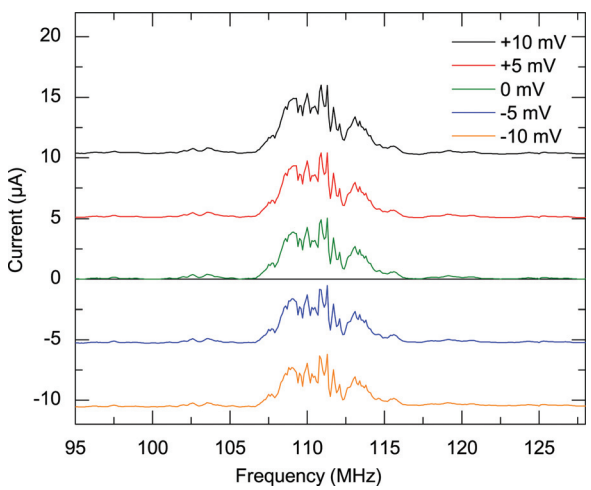

FIG. 5. Acoustoelectric current generated by IDT1 across device 4 as a function of applied biases, demonstrating simultaneous acoustoelectric current with charge counter-flow induced by the applied DC bias.

the region (see Table I in Ref. 19). The magnitude of acoustoelectric current is expected to be proportional to the width of the graphene in the acoustic beam path, as for semiconductor LDSs.[3] This was observed, comparing the data from devices 2 and 4 (contacts 2-3), which had similar resistances ($\sim$1 kΩ) and SAW insertion loss (~ -16 dBm), but different graphene widths. In device 4 the width was 100 μm (defined by lithography and etching), whereas in device 2 the width was estimated to be $\sim$300 μm (the width of unetched graphene in the acoustic beam path). The highest acoustoelectric current for device 4 was 4.98 μA, whereas for device 2 it was 9.88 μA, roughly twice as high.

The origin of the acoustoelectric current can be attributed to the transport of charge carriers by the electric fields which accompany the acoustic waves travelling along the surface of the piezoelectric substrate. As a result of momentum transfer from SAW to the charge carriers, increase in wave attenuation can be expected.

The demonstration of an acoustoelectric effect in graphene paves the way for the acoustic investigation of many transport effects. One example could be that carrier confinement produced by etching may allow experiments analogous to the current pump work performed in semiconductor nanostructures. An intriguing possibility is that if top gating or in-plane gating can be used to change carrier type, then the directed transport of both single-electrons and holes could be obtained in the same nanostructure. The absence of a back gate (lithium niobate being highly insulating) precluded change in the carrier type in the current experiments, but we anticipate that acoustoelectric transport of electrons could be achieved in suitably gated devices. Adjustment of carrier concentration in graphene with the use of gates could also allow *in situ* measurements of changes in SAW attenuation caused by the transfer of SAW momentum to the charge carriers.

In conclusion, we have demonstrated acoustoelectric current flow in graphene films induced by SAWs on lithium niobate. We anticipate that the technique could find widespread application as an effective means to transport charge carriers in graphene.

We gratefully acknowledge useful conversations on device fabrication with S. D. Johnson and C. D. Wood, and funding from EPSRC, the Royal Society, and the Wolfson Foundation.

[1]R. L. Willett, R. R. Ruel, M. A. Paalanen, K. W. West, and L. N. Pfeiffer, Phys. Rev. B **47**, 7344 (1993).
[2]J. M. Shilton, V. I. Talyanskii, M. Pepper, D. A. Ritchie, J. E. F. Frost, C. J. B. Ford, C. G. Smith, and G. A. C. Jones, J. Phys.: Condens. Matter **8**, L531 (1996).
[3]J. M. Shilton, D. R. Mace, V. I. Talyanskii, M. Y. Simmons, M. Pepper, A. C. Churchill, and D. A. Ritchie, J. Phys.: Condens. Matter **7**, 7675 (1995).
[4]J. Cunningham, V. I. Talyanskii, J. M. Shilton, M. Pepper, A. Kristensen, and P. E. Lindelof, Phys. Rev. B **62**, 1564 (2000).
[5]J. Cunningham, M. Pepper, V. I. Talyanskii, and D. A. Ritchie, Appl. Phys. Lett. **86**, 152105 (2005).
[6]N. E. Fletcher, J. Ebbecke, T. J. B. M. Janssen, F. J. Ahlers, M. Pepper, H. E. Beere, and D. A. Ritchie, Phys. Rev. B **68**, 245310 (2003).
[7]C. Rocke, S. Zimmermann, A. Wixforth, J. P. Kotthaus, G. Böhm, and G. Weimann, Phys. Rev. Lett. **78**, 4099 (1997).
[8]O. D. D. Couto, S. Lazic, F. Iikawa, J. A. H. Stotz, U. Jahn, R. Hey, and P. V. Santos, Nature Photon. **3**, 645 (2009).
[9]M. Kataoka, M. R. Astley, A. L. Thorn, D. K. L. Oi, C. H. W. Barnes, C. J. B. Ford, D. Anderson, G. A. C. Jones, I. Farrer, D. A. Ritchie *et al.*, Phys. Rev. Lett. **102**, 156801 (2009).
[10]S. Hermelin, S. Takada, M. Yamamoto, S. Tarucha, A. D. Wieck, L. Saminadayar, C. Bauerle, and T. Meunier, Nature **477**, 435 (2011).
[11]R. P. G. McNeil, M. Kataoka, C. J. B. Ford, C. H. W. Barnes, D. Anderson, G. A. C. Jones, I. Farrer, and D. A. Ritchie, Nature **477**, 439 (2011).
[12]V. I. Talyanskii, D. S. Novikov, B. D. Simons, and L. S. Levitov, Phys. Rev. Lett. **87**, 276802 (2001).
[13]J. Ebbecke, C. J. Strobl, and A. Wixforth, Phys. Rev. B **70**, 233401 (2004).
[14]P. Thalmeier, B. Dóra, and K. Ziegler, Phys. Rev. B **81**, 041409 (2010).
[15]R. Arsat, M. Breedon, M. Shafiei, P. G. Spizziri, S. Gilje, R. B. Kaner, K. Kalantar-zadeh, and W. Wlodarski, Chem. Phys. Lett. **467**, 344 (2009).
[16]D. Čiplys, R. Rimeika, V. Chivukula, M. S. Shur, J. H. Kim, and J. M. Xu, in *2010 IEEE Sensors* (IEEE, New York, 2010), pp. 785–788.
[17]X. Li, W. Cai, J. An, S. Kim, J. Nah, D. Yang, R. Piner, A. Velamakanni, I. Jung, E. Tutuc *et al.*, Science **324**, 1312 (2009).
[18]X. Li, Y. Zhu, W. Cai, M. Borysiak, B. Han, D. Chen, R. D. Piner, L. Colombo, and R. S. Ruoff, Nano Lett. **9**, 4359 (2009).
[19]See supplemental material at http://dx.doi.org/10.1063/1.3697403 for details of the other fabricated devices.
[20]A. C. Ferrari, J. C. Meyer, V. Scardaci, C. Casiraghi, M. Lazzeri, F. Mauri, S. Piscanec, D. Jiang, K. S. Novoselov, S. Roth *et al.*, Phys. Rev. Lett. **97**, 187401 (2006).
[21]M. Rotter, A. Wixforth, W. Ruile, D. Bernklau, and H. Riechert, Appl. Phys. Lett. **73**, 2128 (1998).